Contents lists available at http://qu.edu.iq

Al-Qadisiyah Journal for Engineering Sciences

Journal homepage: https://qjes.qu.edu.iq

The effect of ribs spacing on heat transfer in rectangular channels under the effect of different types of heat flux in the Presence of a nanofluids

Haneen M. Al-Ali[*] and Naseer H. Hamza

Department of Mechanical Engineering, College of Engineering, University of Al-Qadisiyah, Ad-Diwaniyah,58001, Iraq

ARTICLE INFO

ABSTRACT

In this study, numerical computations of the influence of adding ribs in a rectangular channel on the forced convection heat transfer and laminar fluid flow characteristics have been carried out. The analysis was carried out by using the finite element method to solve the dimensionless governing equations for the two-dimensional channel with 80 mm height and 2000 mm length at the Reynolds number of (10, 100, and 500), rib height e=8mm with different aspect ratios (AR =2.5, 3.125, 3.75, 4.375, and 5). Also, the study compared two cases of investigations with and without nanofluid (Water/ TiO2) at the volume fractions of nanoparticles of 0, 2 and 4%. The results concluded that, for certain arrangements, the use of extended surfaces within a rectangular channel can significantly enhance the rate of heat transfer and when the aspect ratios decreases, the Nusselt number increased. However, the existence of ribs within channel in case of constant heat flux can cause a significant improvement of heat transfer compared to that in the corresponding channel under the variable heat flux.

1. Introduction

The use of artificial roughness on a surface in the form of repeated ribs is one of the passive ways to improve the rate of heat transfer. Heat transfer applications have recently become increasingly essential in industrial engineering fields as heat exchangers, power generation, chemical processes, medical applications, air conditioning, electronic devices and solar collectors, etc. [1-4].In past studies, there were many geometric shapes of the ribs which have been studied [5-8]. Among these studies, when using Reynolds number 31170 show the influence of the ribs to improving the heat transfer rate about 213% compared with the smooth surface by Al-taie et al. [9]. Also, the forced convection in the grooved channel has taken the researcher's attention lately [10-12]. On the other hand nanotechnology with dispersing solid particles in a base fluid has been serving as coolants with a view to increases the thermal conductivity of fluid [13, 14]. The thermal conductivity of Al2O3 and SiO2–water nanofluids was measured by Salman et al. [15].The investigation results showed 22% enhancement of heat transfer when using nanofluids. On the other hand, many researchers have presented several reviews in order to show improved viewpoints and states for improving equipment heat transfer [16-18]. Also, another researchers focused on using both method of heat transfer (rough surfaces and nanofluids) [19].

* Corresponding author.
  E-mail address: mech.post05@qu.edu.iq (Haneen M. Al-Ali)

Nomenclature

Cp	specific heat (J kg^{-1} K^{-1})		*Greek symbols*	
D_h	hydraulic diameter of channel (mm)		α	thermal diffusivity (m^2 s^{-1})
k	thermal conductivity (W m^{-1} K^{-1})		υ	kinematics viscosity (m^2 s^{-1})
H	channel height (mm)			solid volume fraction
W	channel width (mm)		φ	
L	total length of the channel (mm)		Θ	dimensionless temperature
L_1	inlet length of the channel (mm)			
L_2	test length of the channel (mm)			
L_3	outlet length of the channel (mm)			
L	dimensionless length, L=l/H			
Nu_x	local Nusselt number		μ	dynamic viscosity (kg m^{-1}s^{-1})
			ρ	density (kg m^{-3})
Nu	average Nusselt number		ΔT	Temperature difference
p	pressure (kg m^{-1} s^{-2})		*Subscripts*	
h	heat transfer coefficient (W m^{-2}K^{-1})		ave	average
Pr	Prandtl number		a	ambient
Re	Reynolds number		c	cold, constant
T	dimensional temperature		f	fluid (pure water)
u	dimensional velocity component in x-direction (m s^{-1})			
v	dimensional velocity component in y-direction (m s^{-1})			
U	non-dimensional velocity component in X-direction		AR	Aspect ratio
V	non-dimensional velocity component in Y-direction		nf	nanofluid
A	Area (m^2)		s	solid nanoparticles
x	dimensional x-coordinate (mm)			
y	dimensional y-coordinate (mm)			
X	non-dimensional X-coordinates		v	variable
Y	non-dimensional Y-coordinates		i	Inlet
e	rib height (mm)		o	outlet
s	rib land/length (mm)			
P	rib pitch (mm)			
(P/e)	Aspect ratio			
ΔP	pressure drop (kg m^{-1} s^{-2})			
q	heat flux (W m^{-2})			

Andreozzi et al. [20] numerically investigated the enhancement of heat transfer of nanofluid flow in a heated channel using various types of ribs. liu et al. [21] performed an experimental and computational study of the thermal performance enhancement in a rectangular passage with perforated ribs. They observed the local heat transfer enhanced due to perforated ribs around 12-24%, and the overall heat transfer increased by 4-8% when compared with the normal ribs.

Chtourou et al. [22] numerically studied the influence of the obstacles on the thermal efficiency inside narrow channels of a plate heat exchangers. With a Reynolds number range 200-800, they investigated and analyzed the impact of the shapes and arrangements of the ribs on hydrothermal behavior. Compared to the smooth duct, the thermal performances are enhanced. They found due to the presence of the obstacles; the heat transfer rate improves from 1.44 to 2.6 times when compared to the smooth case. In the other study, the design of pin-fin heat sink was studied numerically and experimentally by Rezaee et al.[23] Different geometrical parameters of pin-fin were tested in the heat sink. They concluded for all arrangements of pin-fin heat sink that the overall hydrothermal performance significantly increases compared with the smooth case. Wang et al.[24] numerically studied the impact of truncated ribs on the heat transfer and laminar flow characteristics in a ribbed microchannel. The effects of various geometrical parameters (rib width, rib arrangement, and truncation gap height) on hydrothermal performance had been analyzed.

The findings showed that the truncated ribs with the same rib arrangement and width can exhibit better thermal behavior than the continuous ribs case, with decreasing the pressure drop in microchannel. Also, a numerical study by Yadav and Bhagoria [25] found that the flow field, average Nusselt number, and overall hydrothermal performance are all highly influenced by the relative roughness height.

In this study, the influence of change in aspect ratio of extended surfaces, the volume percentage of nanoparticles and Reynolds number are investigated on the behavior heat transfer and laminar flow in a 2-D rectangular channel under two cases of applied heat flux, the first one constant and in the second case is a variable. For the simulation, Reynolds numbers 10, 100, and 500 were used, with nanoparticle concentrations of 0, 2, and 4%, respectively.Up to best knowledge of the authors, very few previous studies discussed the effect of variable heat flux on the flow characteristics in ribbed channels. Also more attention was paid to microchannels, while this study conducted to ordinary channel. In addition to that the optimum value of the aspect ratios as well as the best scenario of heat flux will be presented in current study using numerical approaches. As a result, more data is presented here with a presence of water–TiO$_2$ nanofluid as a coolant to show the heat transfer characteristics of the extended surfaces with different values of aspect ratios.

2. Problem description

The two-dimensional ribbed channel with 10 periodic ribs along the lower wall has been considered in this research as shown schematically in Fig. 1. The total length and the height of the horizontal rectangular channel are set to be L=2000 mm and H=80 mm, respectively. The bottom wall with the length of inlet (L_1=1260 mm) and the length of exit (L_3=200 mm) are insulated, but middle section with the length of (L_2=540mm) is under the effect of heat flux q. The test section has (ten) ribs with height of (e=8), and length of (s=10) for each rib and the space between them varies according to aspect ratio AR. Table 1 explains all of the parameters and measurements shown in Fig. 1
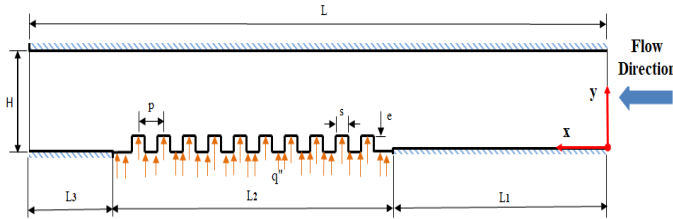

Figure 1. Schematics diagram of rectangular channel.

Table 1. Dimensions of various geometric parameters

Parameter	L (mm)	L_1 (mm)	L_2 (mm)	L_3 (mm)	H (mm)	D_h (mm)	e (mm)	s (mm)	P (mm)
Value dimension	2000	1260	540	200	80	78	8	10	20,25,30,35,40

The working fluid is water and nano-particles, they are added at volume fraction φ= 0, 0.02, 0.04 to explore the effect of adding them with interaction with different geometries which gives a chance to specify the best and optimum combination. The assumptions regarding the working fluid are as follows:

• Incompressible and Newtonian,
• Single phase,
• The co-existing with nano-particles is in thermal and hydraulic equilibrium,
• The physical properties are weak function of temperature and thus approximately constant over the operating range of temperatures' case study.

The applied heat flux is considered at two cases:

Case I: Constant heat flux
In this case the lower wall of channel is exposed to a uniform heat flux condition (q_c =1000 W/m2) on the middle section (test section); while the upper and other remaining walls are insulated.

Case II: Variable heat flux
The lower wall of the test section in this case is subjected to a variable heat flux q(x), the heat flux various linearly according to the equation as:

q(x)=q$_0$+A.x

Where the constants q$_0$, and A will be chosen in such a way that the total heat flux in both cases (constant heat flux and variable heat flux) will be the same. At the inlet section, different fluid velocities are set, and they vary to ensure laminar flow with Reynolds numbers of (10, 100, and 500) but the exits were set to pressure outlet. The inlet temperature is introduced T_c=290K. The thermophysical properties of base fluid and the TiO$_2$ nanoparticles are presented in Table 2.

Table 2. Thermophysical properties of water and solid nanoparticles TiO$_2$ [26].

Material	ρ (kg/m^3)	C_p (J/kg K)	k(W/mk)	μ (Pa s)
Pure water	997.1	4179	0.613	0.001
TiO$_2$	4250	686.2	8.9538	---

3. Mathematical model

In this study, the continuity, momentum, and energy equations of the laminar and steady state forced convection of the Newtonian nanofluid in the channel can be written in dimensional form as follows[27]:

$$\frac{\partial u}{\partial x} + \frac{\partial v}{\partial y} = 0 \tag{1}$$

$$u\frac{\partial u}{\partial x} + v\frac{\partial u}{\partial y} = -\frac{1}{\rho_{nf}}\frac{\partial p}{\partial x} + \frac{\mu_{nf}}{\rho_{nf}}\left(\frac{\partial^2 u}{\partial x^2} + \frac{\partial^2 u}{\partial y^2}\right) \tag{2}$$

$$u\frac{\partial v}{\partial x} + v\frac{\partial v}{\partial y} = -\frac{1}{\rho_{nf}}\frac{\partial p}{\partial y} + \frac{\mu_{nf}}{\rho_{nf}}\left(\frac{\partial^2 v}{\partial x^2} + \frac{\partial^2 v}{\partial y^2}\right) \tag{3}$$

$$u\frac{\partial T}{\partial x} + v\frac{\partial T}{\partial y} = \alpha_{nf}\left(\frac{\partial^2 T}{\partial x^2} + \frac{\partial^2 T}{\partial y^2}\right) \tag{4}$$

The following dimensionless parameters can be used to transform the above governing equations into non-dimensional forms[28]:

$$x = \frac{x}{D_h}, Y = \frac{y}{D_h}, U = \frac{u}{u_i}, V = \frac{v}{u_i}, p = \frac{\bar{P}}{\rho_{nf}u_i^2}$$

$$\theta = \frac{T - T_i}{\Delta T}, Re = \frac{u_i \times D_h}{\nu_f}, Pr = \frac{\nu_f}{\alpha_f}, \Delta T = \frac{q^{"}D_h}{K_f} \tag{5}$$

For steady state and laminar flow, the dimensionless governing equations of continuity, momentum, and energy are expressed as follows: [29]:

$$\frac{\partial U}{\partial X} + \frac{\partial V}{\partial Y} = 0 \tag{6}$$

$$U\frac{\partial U}{\partial X} + V\frac{\partial U}{\partial Y} = -\frac{\partial P}{\partial X} + \frac{\mu_{nf}}{\rho_{nf}\nu_{nf}}\frac{1}{Re}\left(\frac{\partial^2 U}{\partial X^2} + \frac{\partial^2 U}{\partial Y^2}\right) \tag{7}$$

$$U\frac{\partial V}{\partial X} + V\frac{\partial V}{\partial Y} = -\frac{\partial P}{\partial Y} + \frac{\mu_{nf}}{\rho_{nf}\nu_{nf}}\frac{1}{Re}\left(\frac{\partial^2 V}{\partial X^2} + \frac{\partial^2 V}{\partial Y^2}\right) \tag{8}$$

$$U\frac{\partial \theta}{\partial X} V\frac{\partial \theta}{\partial Y} = \frac{\alpha_{nf}}{\alpha_f}\frac{1}{RePr}\left(\frac{\partial^2 \theta}{\partial X^2} + \frac{\partial^2 \theta}{\partial Y^2}\right) \tag{9}$$

The boundary conditions in dimensionless form are described as follows:

U=1, V=0   and $\theta = 0$ for X=0 and 0≤ Y ≤1   (10)

V=0   and $\frac{\partial U}{\partial x} = \frac{\partial \theta}{\partial x} = 0$ for X=2.56 and 0≤ Y ≤1   (11)

V=0, U=0　　and $\frac{\partial\theta}{\partial Y}=0$ or $\frac{\partial\theta}{\partial Y}=-\frac{k_f}{k_{nf}}$　for Y=0 and $0\leq X\leq 2.56$　(12)

V=0, U=0　　and $\frac{\partial\theta}{\partial Y}=0$ for Y=1 and $0\leq X\leq 2.56$　　　(13)

Nanofluid properties of the nanofluid can be defined based on the properties of the base fluid and nanoparticles[30]:

$$\rho_{nf=}(1-\emptyset)\rho_f+\emptyset\rho_s \tag{14}$$

$$(\rho Cp)_{nf}=(1-\emptyset)(\rho Cp)_f+\emptyset(\rho Cp)_s \tag{15}$$

$$\mu_{nf}=\frac{\mu_f}{(1-\emptyset)^{2.5}} \tag{16}$$

$$\frac{K_{nf}}{K_f}=\left[\frac{\left(K_s+2K_f\right)-2\emptyset\left(K_f-K_s\right)}{\left(K_s+2K_f\right)+\emptyset\left(K_f-K_s\right)}\right] \tag{17}$$

The following formulae are used to calculate the local and average Nusselt number [31]:

$$Nu(x)=\frac{h(x).D_h}{K_f}\ ,h(x)=\frac{q^{"}}{T-T_{in}}\longrightarrow q^{"}=\frac{k_f\times\Delta T}{D_h}$$

$$\therefore Nu(X)=\frac{\left(\frac{q^{"}}{T-T_{in}}\right).D_h}{K_f}=\frac{D_h\times K_f\times\Delta T}{K_f\times(T-T_{in})\times D_h}=\frac{\Delta T}{T-T_{in}}$$

$$\longrightarrow Nu(X)=\frac{1}{\theta} \tag{18}$$

$$Nu_{ave}=\frac{1}{L}\int_0^1 Nu(X)dX \tag{19}$$

The following relationship can be used to calculate the pressure drop (P) between the inlet and exit sections. [32]:

$$\Delta P=\bar{P}_{out}-\bar{P}_{in} \tag{20}$$

4. Numerical procedure

In this study, to acquire the surface heat flux distribution of the test section of cooling channel, a numerical procedure was executed using finite element method. Therefore, the laminar two-dimensional Navier-Stokes equations for fluid flow and heat transfer analysis have been solved and discretized numerically combined with the continuity equation and the energy equation with appropriate boundary conditions. The boundary conditions were illustrated in previous paragraph.

5. Validation of the numerical model

In order to check the validity and accuracy of procedure for this numerical study. Current results have been validated by comparing them with a previous study. Fig. 2 shows the validation of the present study with Behnampour et al. [22]. Where it can be concluded from Fig. 2-(a) that the values of the local Nusselt number for the current study correspond to the values of the reference at *Re*=1 and φ=0.04, also Fig. 2-(b) indicates a good matched in the findings for the average Nusselt number.
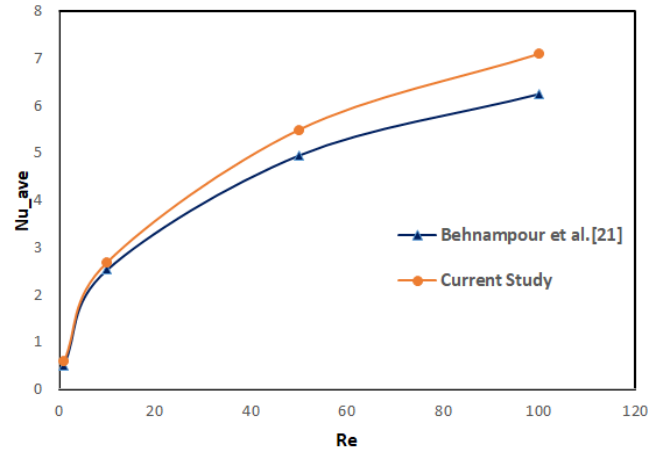
(a)
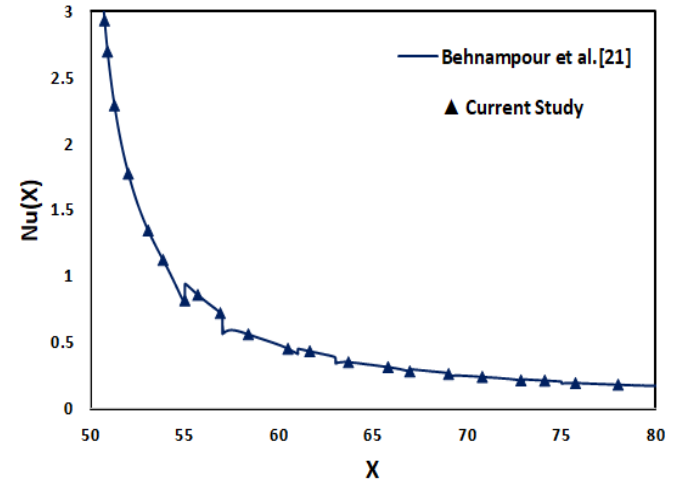
(b)

Figure 2: Validation of present study with Behnampour et al [28]. (a)Local Nusselt number (b) Average Nusselt number

5.1. Gri dindependence test

A grid-independence test is performed to assess the effects of grid sizes on the accuracy and validity of numerical findings.
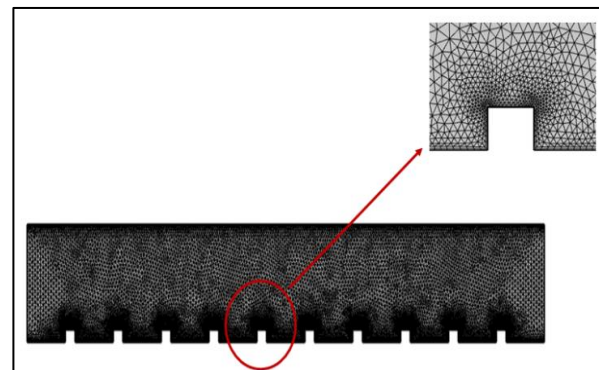

Figure 3. The distribution of triangular mesh

To choose the suitable grid, the average Nusselt number along the lower hot wall of channel for different mesh sizes is estimated. The grid-independence study of the current numerical simulation is performed for ribbed channel with case I (constant heat flux) which is AR=2.5, Re=10 and φ=0.04. As can be shown in Table 3, the optimal mesh for ribbed channel in terms of accuracy and solution time is the Normal grid of (35776). The unstructured triangular meshes for rectangular ribbed channel which used in the present study are shown in Fig. 3.

Table 3. The investigation of grid independency for AR= 2.5, Re=10, and φ=0.04.

Type of Mesh	No. of nodes	Nu-$_{ave}$	Deviation in percentage 100%
Coarser	12330	2.9969	---
Coarse	23125	2.9889	0.26
Normal	35776	2.9879	0.033
Fine	63242	2.9862	0.056
Finer	142707	2.9857	0.016

6. Results and discussion

Figure 4 indicates the dimensionless isotherms diagrams along the rectangular channel for two cases of heat flux in different aspect ratios with Reynolds number of 500 and a volume fraction (φ) of 4%. As seen from the isotherms lines shown in figures below, more changes are created in the form of non-dimensional temperature contours as the AR ratio is increased, due to more energy transferred across the boundaries. In all rib aspect ratios, using high volume fraction of TiO2 nanoparticles causes improvement of heat transfer since the improved thermal conductivity after addition of nano-material to the base fluid and because of the role of solid particles in transferring and conducting the heat energy. When a fluid with a certain temperature comes into contact with rib-roughened hot channel surfaces, the high surfaces temperature lowers, and heat transfer between the hot surfaces and the flowing fluid occurs which increases the fluid temperature by convection and by conduction at very close fluid layers touching the hot ribbed surface. The heat transfer rate increases as the Reynolds number decreases. The reason for this is because when Re is lower, the fluid stays in touch with the hot surface for longer period of time, so absorbing more heat as it passes through the boundary. Ribs along the test section of channel can generate turbulence and so function as mixer and lower the temperature difference between the surface and the fluid, improving heat transmission.
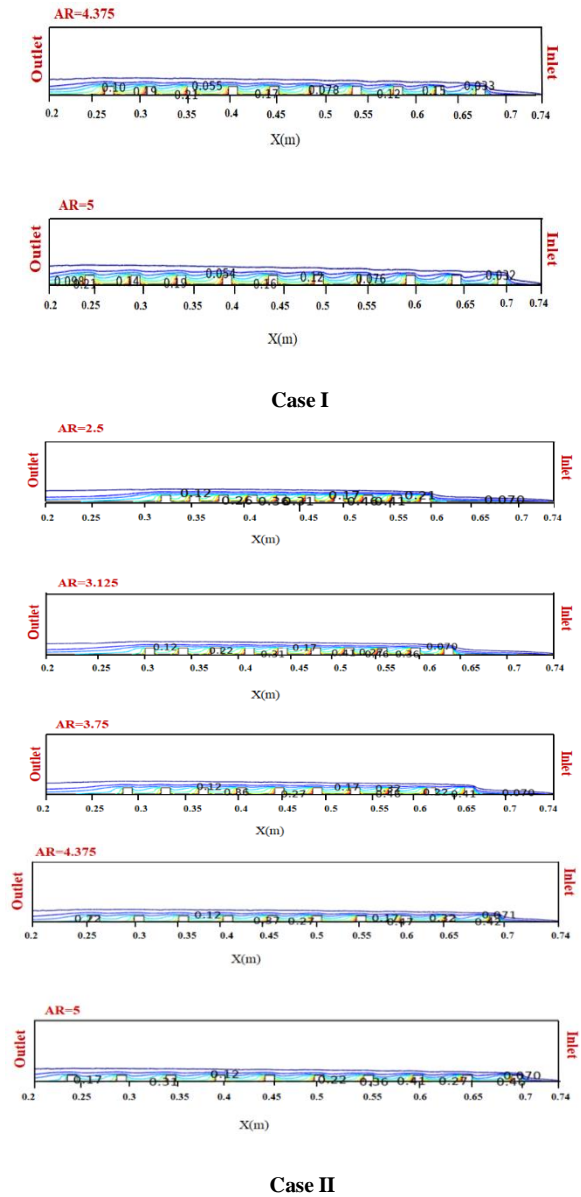

Case I

Case II

Figure 4. Isotherms contours at Re=500 and φ=0.04 for case I (uniform heat flux), and case II (variable heat flux).
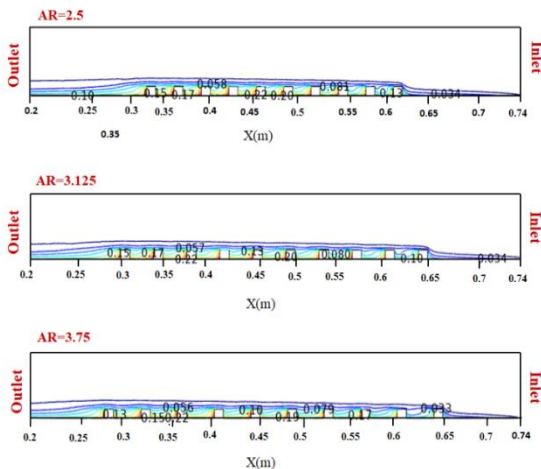
Fig. 5 depicts the streamline contours for two heat flux scenarios using Reynolds numbers of 500 and a volume fraction percentage of 4%. The levels of dimensionless velocity for each rib aspect ratio have been compared According to the diagrams below. As the spaces between extended surfaces and Reynolds number increases, multiple circulations occur in a single space, temperature distribution will be improved due to continuous thermal boundary layer towards the channel centerline. The changes in dimensionless velocity contours will be different in all of the pitch-to-height ratios, and by increasing the rib pitch to higher values, the fluid momentum depreciation in the indentation areas will be significant. This means that changing aspect ratios causes changes in the flow's hydrodynamic behavior.
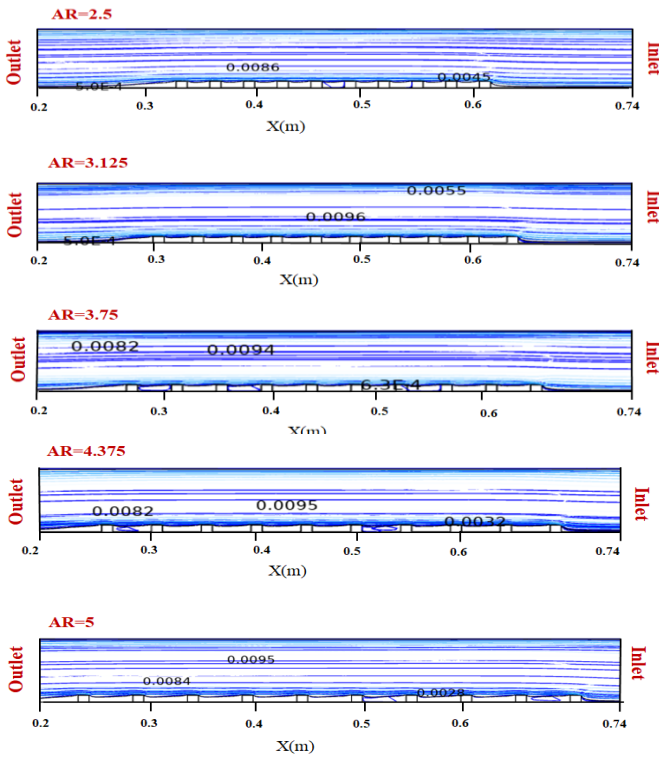
Figure 5. Streamlines contours at *Re*=500 and φ=0.04 for two cases of heat flux.

Fig. 6 shows for case I the variation of average Nusselt number in the aspects ratio for different Reynolds numbers and different volume fractions of solid nanoparticles (0, 2, and 4%). The convection heat transfer for all pitch ratios enhance with the rise of Reynolds number. Among the studied aspect ratios, *AR* =5 has the largest amount of average Nusselt number at *Re* = 10 and *Re* = 100, while at *Re*=500, the largest amount of average Nusselt number is achieved at *AR* =3.75, while *AR* = 2.5 has the minimum amount at all Reynolds numbers. Furthermore, Increasing the Reynolds number also causes eddy flows, which improves the convection heat transfer coefficient. As well as when compared behavior, it is observed that nanofluid has a greater value of Nusselt number compared to pure water. This rise is due to the presence of nanoparticles which causes to increased thermal conductivity of ordinary fluid, also due to effect the Brownian motion of nanoparticles on the enhance the thermal conductivity of nanofluid. Nusselt number improves as nanopartical concentration increase.
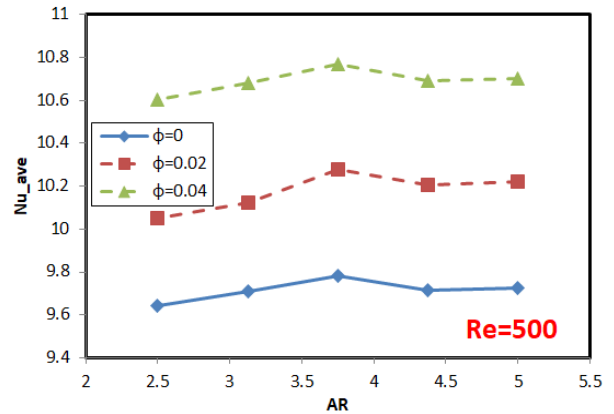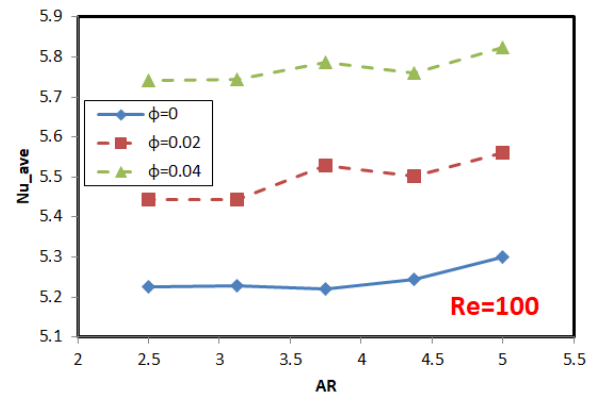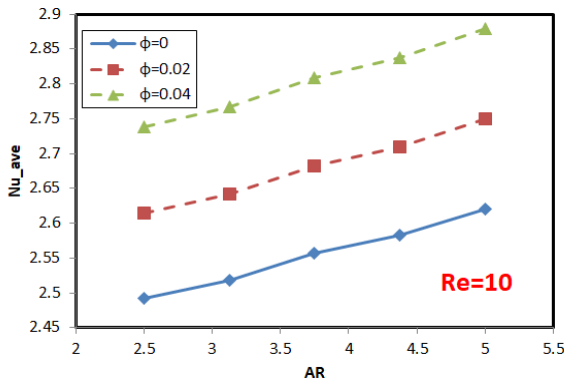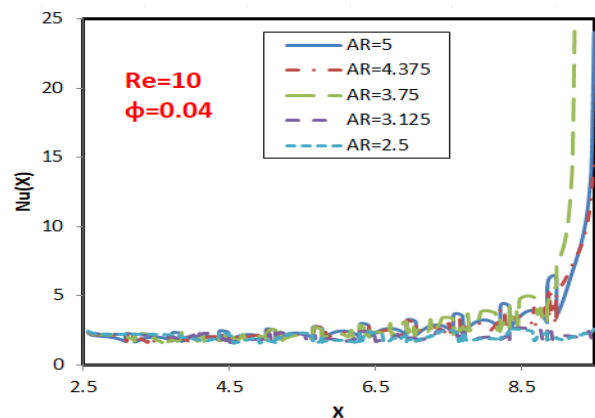

Figure 6. Average Nusselt number versus aspects ratios at different values of Reynolds No. and volume fractions (Case I).

Fig. 7 demonstrates the local Nusselt number along the ribbed channel for case (1) for all spacing values with various values of *Re* and φ=0.04. The local Nusselt number is increased for all aspect ratios with increased values of Reynolds number. Because of the low velocity at *Re*=10, the presence of ribs has no obvious effect on the fluid. In the next schematics, the maximum changes in hydrothermal behavior occur when the fluid collides with the ribs. As a result, the local Nusselt number along the first ribs shows the greatest changes. The first rib produces the most fluctuations at Reynolds numbers of 100 and 500, due to the increased fluid velocity, but the fluctuations decrease as the ribs progress.
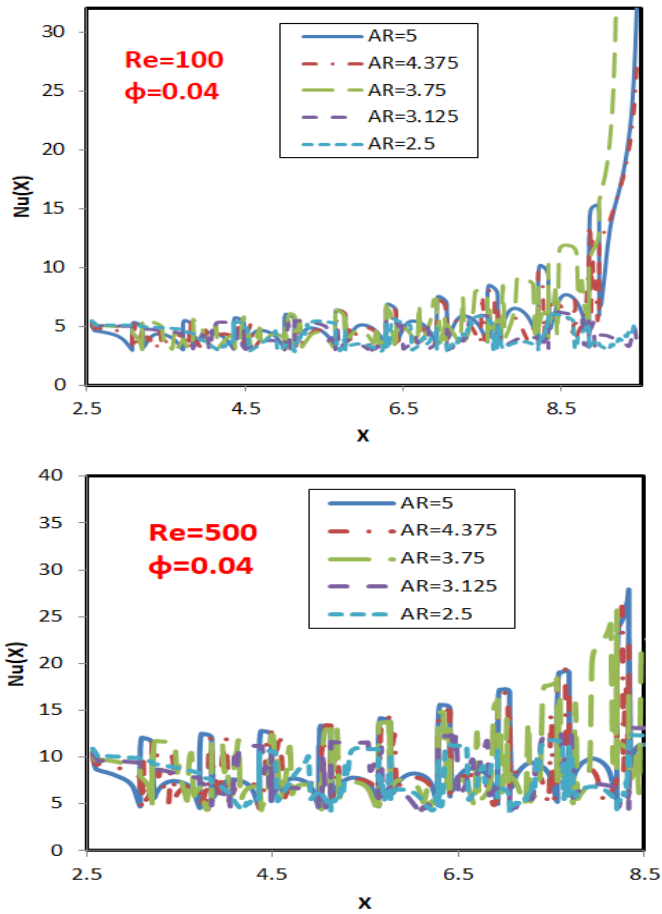
through the ribs, the thermal boundary layers are disturbed and altered, resulting in an increase in heat transfer rate. At mentioned figure, when the nanofluid reaches the left wall of the channel, a fluctuation in the local Nusselt number can be seen in order to recirculate flow in the groove between the ribs, since the graph below has seen a dramatic decrease in the local Nu due to impinging the flow to the rib wall, demonstrating the effect of ribbed channel on heat transfer.

Figure 7. Local Nusselt number in aspects ratio at different values of *Re* for volume fraction φ=0.04 (CaseI).

Also in the second case, the variations of average Nusselt numbers with aspect ratios at different Reynolds number and various fraction factors of nanoparticles are presented in Fig. 8, with the decrease in rib pitch ratios, the average Nu tends to decrease. It can also be seen in this graph that the average Nu tends to rise with the increase in Re, especially when AR=3.75. The flow becomes detached when the distance between two successive ribs increased. Then, it is attached to the walls again. Thus, the rate of heat transfer is increased. On the other hand, the Nusselt number increases with the increasing of aspect ratio. This can be explained by the existence of a ribs turbulator, which causes increase the surface area of channel and lead to rapid mixing between the core and wall flow, leading to high gradients of temperature, especially at lower pitch ratios. Nanofluids are another factor that contributes into increasing the Nusselt number by increases the thermal conductivity of fluid. The thermal behavior is reinforced by increasing the nanoparticles concentration.

From the Fig. 9, it can be seen in case (2) that the local Nusselt numbers are increased for all aspect ratios with increased values of Reynolds number, and the values of local Nusselt number along channel in high Reynolds number is larger than that at low Reynolds number. This is due to the rapid rising of velocity at wider spaces between ribs. Ribs play a crucial role in boosting local Nu, causing a significant rise in Nusselt number in the rib-roughened channel surface. The fundamental reason for this rise is that fluid layers between cold and hot places are better mixed. When fluid passes
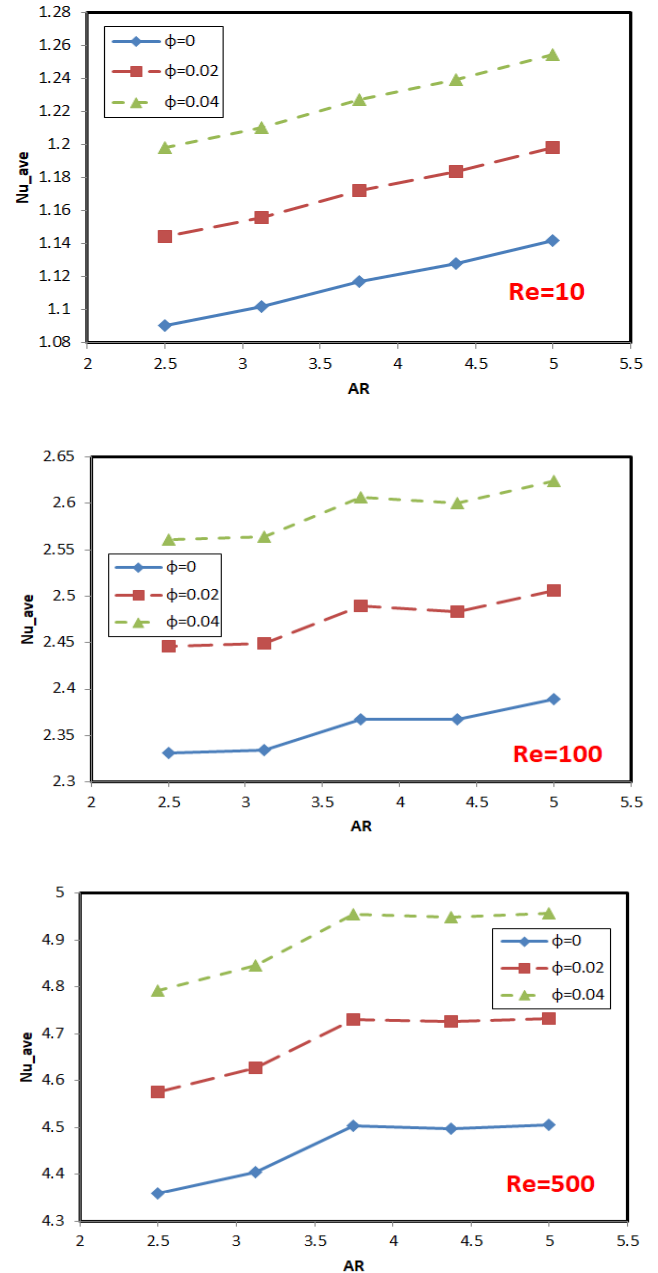

Figure 8. Average Nusselt number versus aspects ratios at different values of Reynolds No. and volume fractions (Case II).
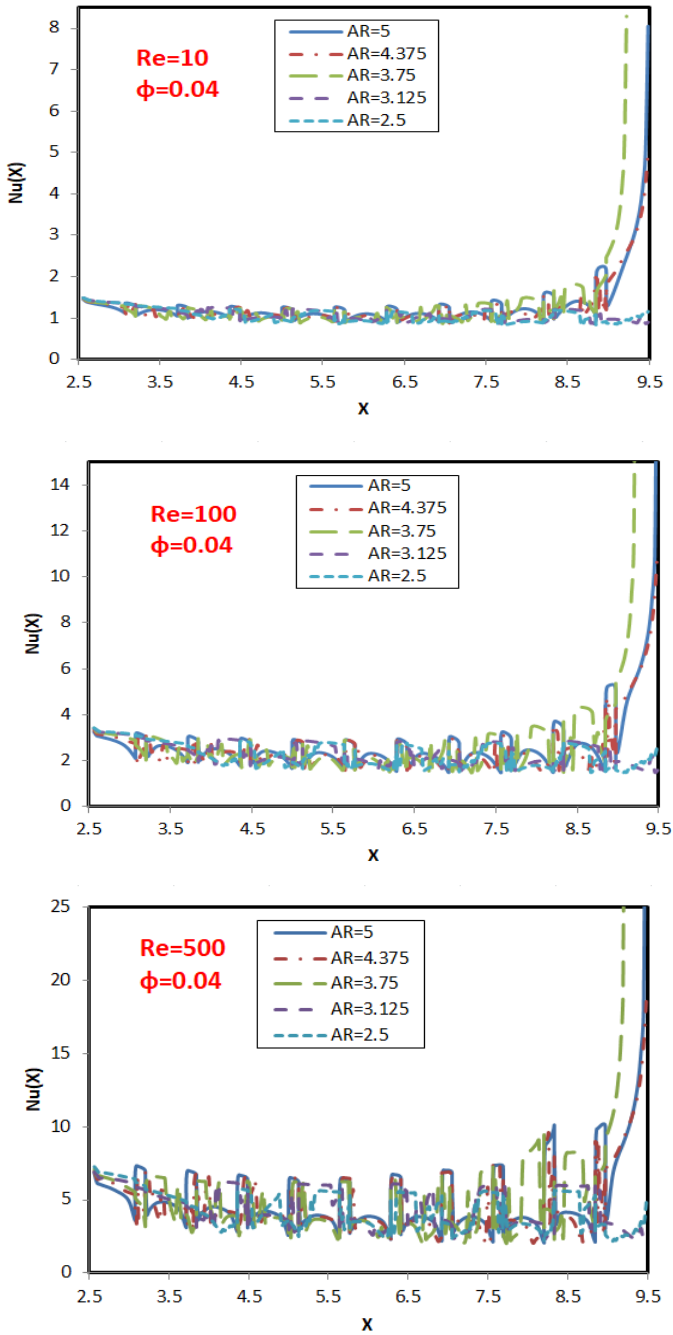
Figure 9. Local Nusselt number in aspects ratio at different values of Re for volume fraction φ=0.04 (Case II).

Table 4 shows the average Nusselt number values for two cases and Reynolds numbers of 10, 100 and 500 with different volume fraction of nanoparticles. These values were calculated on the upper boundaries of the hot ribbed wall, and based on the tabulated results below, the average Nusselt number of $Re = 10$ and $Re=100$ for case I of heat flux and for all percentages for nanoparticle has less changes than those of $Re = 500$, while all are better than the second case II. This is due to an increase in fluid velocity at higher Reynolds numbers, as well as the enhancement of

nanoparticle heat transfer mechanisms by increasing the volumetric percent of suspended nanoparticles in the base fluid.

Table 4. Average Nusselt number of various values of AR under different conditions.

Case of study	Re	φ	Aspect ratios (AR)				
			2.5	3.125	3.75	4.375	5
			Nu_{ave}				
Case I	10	0	2.49	2.51	2.55	2.58	2.62
		0.02	2.61	2.64	2.68	2.71	2.74
		0.04	2.73	2.76	2.80	2.83	2.87
	100	0	5.22	5.22	5.22	5.24	5.30
		0.02	5.44	5.44	5.52	5.50	5.56
		0.04	5.74	5.74	5.78	5.76	5.82
	500	0	9.64	9.70	9.78	9.71	9.72
		0.02	10.04	10.12	10.27	10.20	10.21
		0.04	10.60	10.68	10.76	10.69	10.70
Case II	10	0	1.09	1.10	1.11	1.12	1.14
		0.02	1.14	1.15	1.17	1.18	1.19
		0.04	1.19	1.21	1.22	1.23	1.25
	100	0	2.33	2.33	2.36	2.36	2.38
		0.02	2.44	2.44	2.49	2.48	2.50
		0.04	2.56	2.56	2.60	2.60	2.62
	500	0	4.35	4.40	4.50	4.49	4.50
		0.02	4.57	4.62	4.73	4.72	4.73
		0.04	4.79	4.84	4.95	4.94	4.95

7. Conclusions

The impacts of rib spacing on the laminar forced convection heat transfer of (Water/ TiO2) nanofluid in a two-dimensional rectangular duct under two situations of heat flux boundary condition were investigated in this study using computational fluid dynamics (CFD). The emphasis was given on the heat transfer enhancement resulting from changing parameters include different aspect ratios of ribs (P/e) changing from 2.5 to 5. The influence of the abovementioned parameters on the average Nusselt number for two cases of heat flux are presented and discussed. As a result, the following findings have been achieved:

- The breakdown of the thermal boundary by ribs in a ribbed channel produces mixing enhancement, which results in a rise in the average Nusselt number. Moreover, the average Nusselt number rises with the increase in Reynolds number.
- The heat transfer process in the ribbed channel is affected by the spacing between the extended surfaces. For certain extent, the heat transfer rate increases with the increase in rib pitch.
- Reynolds number of 500 has the largest rate of heat transfer in all instances, whereas Reynolds number of 10 has the lowest rate of heat transmission, which affirms the direct proportional relationship between Nu and Re numbers.

- The Nusselt number was found to be increased as the spacing increased. For this parameter, the case I show better results than case II, because the uniformness and constant distribution of heat transfer rate in all range of Reynolds Number and this result leads to increase of thermal performance factor.
- The maximum value of average Nusselt number is found to be 10.76 for the ratio of pitch to height of rib is 3.75 and volume fraction of 0.04 at a higher Reynolds number 500, in case of constant heat flux (Case I).

Authors' contribution
All authors contributed equally to the preparation of this article.

Declaration of competing interest
The authors declare no conflicts of interest.

Funding source
This study didn't receive any specific funds.

References

[1] T. Venkateshan, M.J.I.J.R.A.S.E.T. Eswaramoorthi, A review on performance of heat exchangers with different configurations, International Journal for Research in Applied Science & Engineering Technology (IJRASET), 3(7) (2015) 1-5.

[2] B. Bhushan, R.J.E. Singh, A review on methodology of artificial roughness used in duct of solar air heaters, Energy, 35(1) (2010) 202-212.

[3] P.M. Aamir, R. Kapadia, D. Deore, Performance Investigation of Automobile Car Radiator using Nano fluid-A Review, International Journal of Science Technology & Engineering, 2(09) (2016).

[4] B.J.S.E. Prasad, Thermal performance of artificially roughened solar air heaters, Solar Energy, 91(May 2013) (2013) 59-67.

[5] G.F.J.I.J.o.E. Smaisim, Environment, Investigation on heat transfer augmentation using continuous and broken ribs on a plate of heat exchanger, ENERGY AND ENVIRONMENT, 9(3) (2018) 211-232.

[6] M.W. Al-Jibory, F.L. Rashid, S.J.I.J.o.M.E. Talib, Technology, An experimental Investigation of Heat Transfer Enhancement in Elliptical Passage Fitted with Different rib Geometries, International Journal of Mechanical Engineering and Technology, 13(9) (2018) 1033-1048.

[7] S. Zheng, T. Ji, G. Xie, B.J.N.H.T. Sundén, Part A: Applications, On the improvement of the poor heat transfer lee-side regions of square cross-section ribbed channels, International Journal of Computation and Methodology, 66(9) (2014) 963-989.

[8] K. Yongsiri, P. Eiamsa-Ard, K. Wongcharee, S.J.C.S.i.T.E. Eiamsa-Ard, Augmented heat transfer in a turbulent channel flow with inclined detached-ribs, Case StudiesinThermalEngineering, 3 (2014) 1-10.

[9] A. Al-taie, H.A.J.J.o.U.o.B. Jurmut, Experimental and Numerical Investigation of Convective Heat Transfer in a Circular Tube with Internal square ribs, Journal of Babylon University/Engineering Sciences, 22(4) (2014).

[10] Y. Li, D.X. Jin, Y.Q. Jing, B.C. Yang, An experiment investigation of heat transfer enhancement by pulsating laminar flow in rectangular grooved channels, in: Advanced Materials Research, Trans Tech Publ, 2013, pp. 74-77.

[11] K. Bilen, M. Cetin, H. Gul, T.J.A.T.E. Balta, The investigation of groove geometry effect on heat transfer for internally grooved tubes, Applied Thermal Engineering, 29(4) (2009) 753-761.

[12] P. Promthaisong, A. Boonloi, W.J.I.J.o.M. Jedsadaratanachai, M. Engineering, Numerical investigation on turbulent forced convection and heat transfer characteristic in spirally semicircle-grooved tube, International Journal of Mechanical and Materials Engineering, 11(1) (2016) 1-15.

[13] S.A. Sajadifar, A. Karimipour, D.J.E.J.o.M.-B.F. Toghraie, Fluid flow and heat transfer of non-Newtonian nanofluid in a microtube considering slip velocity and temperature jump boundary conditions, European Journal of Mechanics B/Fluids, 61(February 2017) (2017) 25-32.

[14] N. Usri, W. Azmi, R. Mamat, K.A.J.I.J.o.A. Hamid, M. Engineering, Forced convection heat transfer using water-ethylene glycol (60: 40) based nanofluids in automotive cooling system, International Journal of Automotive and Mechanical Engineering (IJAME) 11(June 2015) (2015) 2747-2755.

[15] B. Salman, H. Mohammed, A.S.J.I.C.i.H. Kherbeet, M. Transfer, Numerical and experimental investigation of heat transfer enhancement in a microtube using nanofluids, International Communications in Heat and Mass Transfer, 59(December 2014) (2014) 88-100.

[16] N.C. Kanojiya, V. Kriplani, P.J.I.J.o.E.R. Walke, Technology, Heat Transfer Enhancement in Heat Exchangers With Inserts: A Review, International Journal of Engineering Research & Technology (IJERT), 3(10) (2014).

[17] A.R.S. Suri, A. Kumar, R.J.I.J.o.A.E. Maithani, Convective heat transfer enhancement techniques of heat exchanger tubes: a review, International Journal of Ambient Energy, 39(7) (2018) 649-670.

[18] A. Kumar, R. Saini, J.J.R.E. Saini, Heat and fluid flow characteristics of roughened solar air heater ducts–A review, Renewable Energy, 47(November 2012) (2012) 77-94.

[19] S. Kumar, A.D. Kothiyal, M.S. Bisht, A.J.C.S.i.T.E. Kumar, Numerical analysis of thermal hydraulic performance of Al2O3–H2O nanofluid flowing through a protrusion obstacles square mini channel, Case Studies in Thermal Engineering, 9(January 2017) (2017) 108-121.

[20] A. Andreozzi, O. Manca, S. Nardini, D.J.A.T.E. Ricci, Forced convection enhancement in channels with transversal ribs and nanofluids, Applied Thermal Engineering, 98(5 April 2016) (2016) 1044-1053.

[21] J. Liu, S. Hussain, W. Wang, G. Xie, B.J.I.C.i.H. Sundén, M. Transfer, Experimental and numerical investigations of heat transfer and fluid flow in a rectangular channel with perforated ribs, International Communications in Heat and Mass Transfer, 121(February 2021) (2021) 105083.

[22] S. Chtourou, H. Djemel, M. Kaffel, M.J.S.A.S. Baccar, Predicting the effect of the rib pitch on thermal performance factor of small channels plate heat exchangers fitted with Y and C shapes obstacles, Springer Nature journal, 3(4) (2021) 1-28.

[23] M. Rezaee, M. Khoshvaght-Aliabadi, A.A. Arani, S.J.C.E. Mazloumi, P.-P. Intensification, Heat transfer intensification in pin-fin heat sink by changing pin-length/longitudinal-pitch, Chemical Engineering & Processing: Process Intensification, 141(July 2019) (2019) 107544.

[24] G. Wang, T. Chen, M. Tian, G.J.I.J.o.H. Ding, M. Transfer, Fluid and heat transfer characteristics of microchannel heat sink with truncated rib on sidewall, International Journal of Heat and Mass Transfer, 148(February 2020) (2020) 119142.

[25] A.S. Yadav, J.J.N.H.T. Bhagoria, Part A: Applications, A numerical investigation of turbulent flows through an artificially roughened solar air heater, Numerical Heat Transfer, 65(7) (2014) 679-698.

[26] T.-C. Hung, W.-M. Yan, X.-D. Wang, C.-Y.J.I.J.o.H. Chang, M. Transfer, Heat transfer enhancement in microchannel heat sinks using nanofluids, International Journal of Heat and Mass Transfer, 55(9-10) (2012) 2559-2570.

[27] A. Raisi, S. Aminossadati, B.J.J.o.t.T.I.o.C.E. Ghasemi, An innovative nanofluid-based cooling using separated natural and forced convection in low Reynolds flows, Journal of the Taiwan Institute of Chemical Engineers, 62(May 2016) (2016) 259-266.

[28] A. Behnampour, O.A. Akbari, M.R. Safaei, M. Ghavami, A. Marzban, G.A.S. Shabani, R.J.P.E.L.-D.S. Mashayekhi, Nanostructures, Analysis of heat transfer and nanofluid fluid flow in microchannels with trapezoidal, rectangular and triangular shaped ribs, Physica E: Low-dimensional Systems and Nanostructures, 91(July 2017) (2017) 15-31.

[29] O.A. Akbari, D. Toghraie, A. Karimipour, M.R. Safaei, M. Goodarzi, H. Alipour, M.J.A.M. Dahari, Computation, Investigation of rib's height effect on heat transfer and flow parameters of laminar water–Al2O3 nanofluid in a rib-microchannel, Applied Mathematics and Computation, 290(1 November 2016) (2016) 135-153.

[30] J. Lee, I.J.I.J.o.H. Mudawar, M. Transfer, Assessment of the effectiveness of nanofluids for single-phase and two-phase heat transfer in micro-channels, International Journal of Heat and Mass Transfer, 50(3-4) (2007) 452-463.

[31] S. Aminossadati, A. Raisi, B.J.I.J.o.N.-L.M. Ghasemi, Effects of magnetic field on nanofluid forced convection in a partially heated microchannel, International Journal of Non-Linear Mechanics, 46(10) (2011) 1373-1382.

[32] S.M. Vanaki, H.J.I.C.i.H. Mohammed, M. Transfer, Numerical study of nanofluid forced convection flow in channels using different shaped transverse ribs, International Communications in Heat and Mass Transfer, 67(October 2015) (2015) 176-188.